

RESEARCH ARTICLE

 OPEN ACCESS

Received: 01.02.2020

Accepted: 17.11.2020

Published: 08.12.2020

Citation: Langbang D, Dhodapkar R, Premarajan KC (2020) New insight into the In-Silico prediction and molecular docking of *Giardia intestinalis* protease resistance to nitroimidazole. Indian Journal of Science and Technology 13(43): 4434-4445. <https://doi.org/10.17485/IJST/v13i43.100>

* **Corresponding author.**

rahuldhodapkar@gmail.com

Funding: Jawaharlal Institute of Postgraduate Medical Education and Research (JIPMER), Pondicherry, India

Competing Interests: None

Copyright: © 2020 Langbang et al. This is an open access article distributed under the terms of the [Creative Commons Attribution License](https://creativecommons.org/licenses/by/4.0/), which permits unrestricted use, distribution, and reproduction in any medium, provided the original author and source are credited.

Published By Indian Society for Education and Environment ([iSee](https://www.indjst.org/))

ISSN

Print: 0974-6846

Electronic: 0974-5645

New insight into the In-Silico prediction and molecular docking of *Giardia intestinalis* protease resistance to nitroimidazole

Dashwa Langbang¹, Rahul Dhodapkar^{2*}, KC Premarajan³

1 PhD scholar, Department of Microbiology, Jawaharlal Institute of Postgraduate Medical Education and Research (JIPMER), Puducherry, 605006, India

2 Additional Professor, Department of Microbiology, Jawaharlal Institute of Postgraduate Medical Education and Research (JIPMER), Puducherry, 605006, India

3 Professor, Department of Community Medicine, Jawaharlal Institute of Postgraduate Medical Education and Research (JIPMER), Puducherry, 605006, India

Abstract

Background/Objective. *Giardia intestinalis* is a flagella protozoan residing in human intestine causing diarrhea that affecting most common among the children. Usually metronidazole and nitroimidazole were used for the treatment of giardiasis worldwide. Pyruvate Ferredoxin oxidoreductase (PFeO) protease enzyme may play a role inactivation of these drugs that may lead to resistance. Studies regarding drug resistance are very less. Therefore, present study was carried out to predict the structure and characterize them structurally as well as functionally by using appropriate in-silico methods. **Methods:** The proteins sequences of wild type and mutant strain i.e. Pyruvate Ferredoxin oxidoreductase (PFeO) and Pyruvate flavodoxin oxidoreductase (PFIO) were retracted from the NCBI and aligned using ClustalW. Bioinformatic tools were carried out like molecular dynamics simulations and docking to understand the three-dimensional (3D) conformational structure and interaction behavior of mutant and wild types with the ligand. **Findings:** The wild complex maintained an approximate 4H-bonds during simulation while the mutant complex could hardly maintain single H-bond by the end of the simulation, suggesting that 4-nitroimidazole is highly stable in the wild complex. Since the compound occupies this binding site by making stable H-bond with key interacting residues, the function of mutant may be affected. For the very reason, the mutant may be resistant to the nitroimidazole. **Applications:** Molecular dynamic simulation and docking results have increased our understanding of resistance mechanisms and may also help for the design derivatives of nitroimidazole that inhibit protein function more efficiently.

Keywords: Molecular dynamic simulation; Nitroimidazole resistance; Pyruvate Ferredoxin Oxidoreductase (PFeO) mutant type; Pyruvate Flavodoxin Oxidoreductase (PFIO) wild type; *Giardia intestinalis*

1 Introduction

Giardia intestinalis (syn. *Giardia lamblia* or *Giardia duodenalis*) belong to protozoa which are intestinal parasites residing in the small intestine of the human, this parasite causes diarrhea in human and domestic animals as well, while children's is known to be more susceptible to this parasite infection. The infections occurred worldwide, however, they estimated that more than four hundred million cases annually are affecting by this infection and increased with their incidence rate^(1,2). Most commonly seen in the developing countries with a poor hygienic setting, 15% approximately *Giardia* infections mostly occur it is children group which is less than 10 years of age and it considers as the second foremost cause of death in children under five years old^(3–6). Most of the cases were found to be asymptomatic they act as a carrier, but in the symptomatic cases may lead to chronic and acute symptoms which include nausea, diarrhea, dehydration, malabsorption syndrome⁽¹⁾.

G. intestinalis infection can cause like irritable bowel syndrome, it has been found that the infection has some impact on the patient with obesity and type II diabetes^(7,8). Presently worldwide treatment of giardiasis constrained to the nitro heterocyclic group of drugs like metronidazole, nitroimidazole, and furazolidone compounds^(9,10). Some of the studies abroad has been reported that clinical isolates of *Giardia intestinalis* have diverse levels of resistance against these nitro groups of drugs may be due to overexpressing some protease enzymes related to drug resistance^(10–13). But the mechanistic basis for this resistance is not known. It has been reported that the protease enzyme known as pyruvate ferredoxin oxidoreductase (PFo) mutant type which is present in the *Giardia* showed resistance to metronidazole and nitroimidazole drugs by inactivating the activity of these particular drugs⁽¹⁴⁾. The metronidazole inactive oxide form enters the cell of *Giardia* through passive diffusion methods and inside mitochondria organelle of *Giardia* the nitrogen being converted to toxic radicals by reduced pyruvate-ferredoxin oxidoreductase enzyme (PFo) mutant type^(15,16). This mutation in the gene of pyruvate ferredoxin oxidoreductase of *G. intestinalis* can able to decrease the protein binding affinity process which brings down the expression of the protease enzyme and its resistance to nitroimidazole and metronidazole.

Previously various studies regarding nitro heterocyclic drug resistance by *Giardia* has been evaluated in different aspect like regulation of Oxidoreductase enzymes in mRNA expression levels that take place in the parasite^(17–19). However, there are no complete study has been showed at the protein level of replication in *Giardia* which is related to nitro heterocyclic resistance of *G. intestinalis* isolates. In western countries they find it is one of the major problems in treating nitro imidazole-resistant clinical isolates of *Giardia* in the patients, these nitro group of drug their permeability does not alter on the trophozoites and developed cysts of the parasite and there are no significant changes at lower concentrations to stop the multiplication of cyst production of the parasite^(20,21). Pyruvate-ferredoxin oxidoreductase enzyme is known to be involved as nitro-binding protein in drug resistance that presents in *G. intestinalis*. Therefore, resistance to this nitroimidazole drug in *G. intestinalis* may be due to pyruvate ferredoxin oxidoreductase activity of this enzyme,

So, therefore, the present study aimed to understand the drug-resistant mechanism involve in the *G. intestinalis* by using appropriate in-silico bioinformatics tools like simulation and molecular docking of pyruvate-ferredoxin oxidoreductase enzyme with the particular drug ligand nitroimidazole.

2 Materials and Methods

2.1 Homology modeling/template selection and sequence alignment

The protein sequences of mutant and wild types of *Giardia intestinalis* were extracted from National Centre for Biotechnology Information (NCBI) protein search with accession numbers AAA74894.1 and XP_001708948.1, respectively. The Basic Local Alignment Search Tool protein (BLASTp) search was performed to retrieve the most similar template structure for homology modeling⁽²²⁾. Both mutant and wild protein sequences have structural similarity with pyruvate-ferredoxin oxidoreductase protein structure from *Moorella thermoacetica* American Type Culture Collection (ATCC) 39073 with an E-value of 0.0. With this template, the wild protein showed a sequence identity of 47.04% and query coverage of 98% while the mutant protein exhibited a sequence identity of 37.16% and query coverage of 97%. Then, homology modeling was performed to predict the 3D protein structure using the Modeller9v19 script⁽²³⁾. A set of 50 protein models was generated relying on sequence alignment and template structure assuring the spatial constraints. The model with low molecular PDF (mol pdf) score was evaluated with Rampage Ramachandran plot⁽²⁴⁾. The residues lying in the disallowed region were subjected to loop modeling if they are present in the loop region of the protein. Again, a set of 50 models was generated with a loop modeling procedure and the model with the lowest molecular PDF (mol pdf) score was selected for further studies.

2.2 Molecular dynamics (MD) simulation

To analyze the stability of the modeled structure and to extract the minimized structure, Molecular dynamic simulation was performed using GROMACS 5⁽²⁵⁾. The Gromos 43A1 force field was applied and the protein was placed at the geometrical center of the triclinic box with a distance of 1.0 nm from the box edge. The box was solvated with simple point charged (SPC) explicit water molecules. The redundant charge of the system was neutralized with a sufficient amount of counter ions by replacing solvent molecules. Then, the energy minimization of the entire system was done using the steepest descent algorithm with a tolerance force for convergence of <1000.0 kJ/mol/nm. Subsequently, the system was equilibrated with the NVT ensemble using a leap-frog integrator with a time step of 2 fs, where initial velocities were assigned from Maxwell distribution to gradually heat the system to 300K. For temperature coupling, the modified Berendsen or V-rescale thermostat was used with 0.1 ps time constant. The NPT ensemble was then applied using Parrinello-Rahman barostat with 0.2 ps time constant to attain 1bar pressure. All bonds have pertained with LINear Constraint Solver (LINCS) holonomic constraints for van der Waals and electrostatic interactions with 10 Å cut-off⁽²⁶⁾. For long-range electrostatics, the Particle-Mesh-Ewald (PME) coulomb type with a cubic interpolation order of 4 and a grid spacing of 0.16 nm was applied⁽²⁷⁾. Finally, the MD run was performed in the NPT ensemble for a time scale of 10 ns. The same protocol was implemented for protein-ligand simulation while the ligand parameters were obtained from the swissparam server with CHARMM force field⁽²⁸⁾.

2.3 Essential dynamics

The principal component analysis (PCA) and free energy landscape (FEL) were plotted for all four structures i.e., wild, mutant, complex-wild and complex-mutant to attain the minimum energy structure. At first, the covariance matrix was constructed from backbone atomic fluctuations of protein structure by avoiding the removal of rotational and translational movement. The sum of eigenvalues was computed from the diagonalization of the covariance matrix. Then, the detailed analysis of motion was performed along with eigenvector direction by projecting onto individual eigenvectors using gmx anaig. From the analysis, the protein structure with the lowest free energy was extracted from the trajectory for further studies.

2.4 Binding site prediction

The binding site of both wild and mutant types proteins was predicted by Computed Atlas of Surface Topography of proteins (CASTp) server⁽⁶⁾. Both protein structures were submitted to the CASTp server individually in PDB format as input and a probe radius of 2.0 Å was given for computing solvent accessible surface area (SASA).

2.5 Molecular docking

As explained earlier, the protein structure of wild and mutant types was extracted from the FEL plot while the 3D structure of ligand i.e. 4-nitroimidazole was downloaded from PubChem (ID: 18208). Molecular docking was performed using AutoDock to predict the binding pocket of 4-nitroimidazole and to obtain its binding affinity⁽²⁹⁾. Initially, the protein (both wild and mutant) was prepared for docking by adding the polar hydrogens and Kollman charges. In the second step, the ligand was prepared by employing Gasteiger charges⁽³⁰⁾. The prepared protein and ligand files were transformed into pdbqt format that contains atom coordinates, partial charges, and solvation parameters. In the third step, the grid maps were calculated using the AutoGrid program with binding site residues predicted by the CASTp server. At last, the docking was performed using the Lamarckian genetic algorithm (GA) which is an adaptive local search method. During docking, the protein was kept rigid and the torsional bonds of 4-nitroimidazole were allowed to be flexible. Lamarckian GA was employed for a set of 50 generation cycles composed of mapping, fitness energy evaluation for a maximum value of 2.5×10^6 with a selection, crossover and mutation rate of 0.02. The generated conformers were scored by AutoDock energy-based scoring function that includes scoring for H-bond, short-range van der Waals and electrostatic interactions and loss of entropy due to solvation and ligand binding^(30,31). The conformation with the lowest binding energy in the largest cluster was considered for further analysis.

3 Results

3.1 Structural analysis of predicted mutant and wild models

Among the 50 generated models, wild type had the lowest mol pdf value of 6464.68652 and mutant type had a score of 7084.38086. Structure validation (after loop refinement) of wild type by Ramachandran plot showed 95.8% of residues in the favored region, 3.6% residues in allowed and 0.6% residues in the outlier region as shown in (Figure 1). In the case of mutant, 94.6% residues lied in the favored region, 3.9% residues in allowed while 1.4% residues fallen in the outlier region as shown

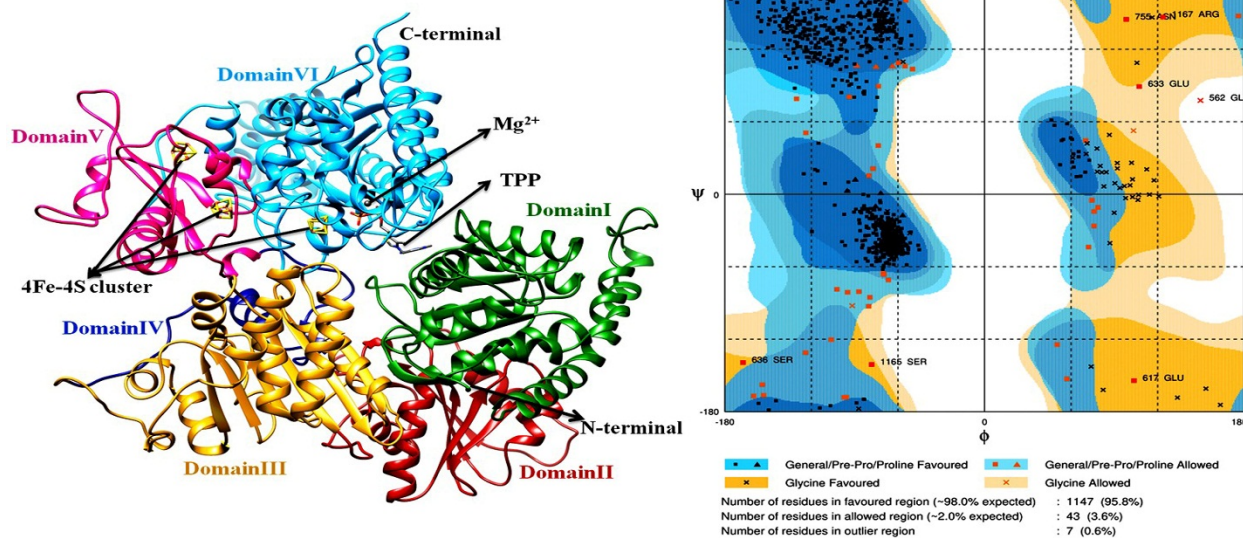


Fig 1. The predicted structure of wild type and arrangement of six domains along with the Ramachandran plot.

in (Figure 2). The structural analysis was performed based on template protein. Both wild and mutant structures composed of six domains, three iron-sulfur [4Fe-4S] clusters, one thiamine pyrophosphate (TPP) and one Mg²⁺ molecule. In wild type, the sequence length for six domains ranged as follows: domain I (1-258), domain II (259-420), domain III (421-641), domain IV (642-685), domain V (686-807) and domain VI (808-1199) as shown in (Figure 1) while in mutant type, the length is as follows: domain I (1-265), domain II (266-440), domain III (441-663), domain IV (664-703), domain V (704-825) and domain VI (826-1253) as shown in (Figure 2). In both types, the domain I interacted with pyrimidine moiety of TPP while domain VI binds with pyrophosphate group of TPP and proximal [4Fe-4S] cluster. The domain II and domain III are similar to the transketolase C-terminal (TKC) domain and coenzyme A (CoA)-binding domain of template. The domain IV is a structural linker that connects domains III and V. The domain V forms ferredoxin fold that accommodated distal [4Fe-4S] cluster and medial to TPP molecule.

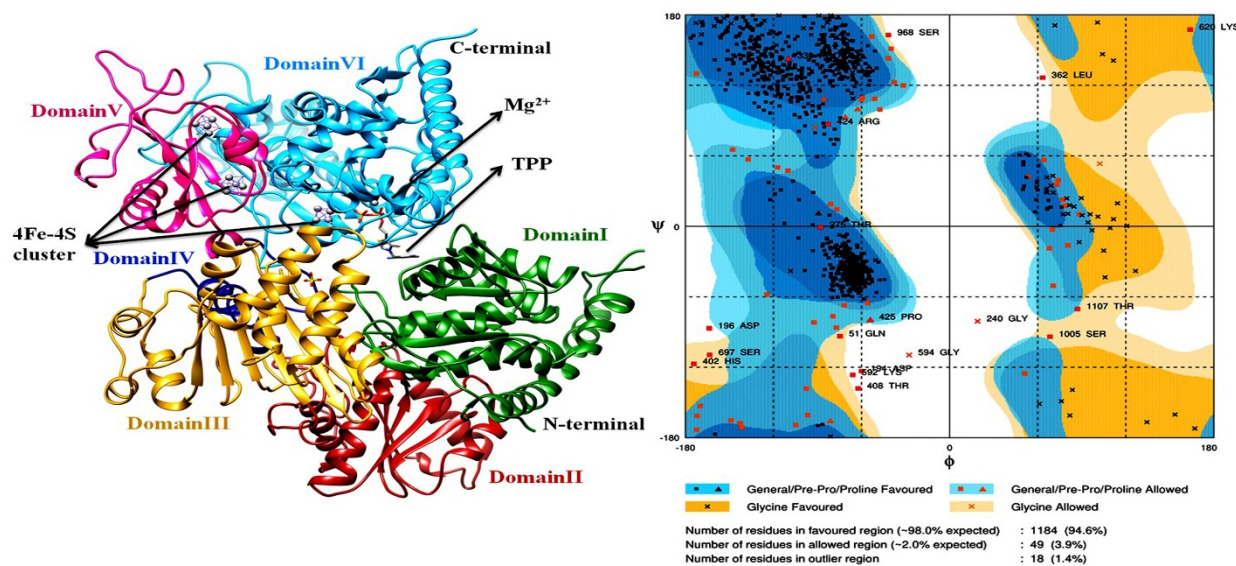


Fig 2. The domain arrangement in predicted mutant type structure and Ramachandran plot for structure validation.

3.2 MD simulation analysis

During the MD simulation, the behavior of protein was studied as a function of time. The root-mean-square deviation (RMSD) plot explains that the wild protein has converged after 6 ns and was quite stable for the rest of the simulation compared to mutant protein simulation as shown in (Figure 3 A). In the root-mean-square fluctuation (RMSF) plot, the highest fluctuation was observed at C-terminus which generally happens due to free end as shown in (Figure 3B). As per the Rg plot, the compactness of both the proteins increased during the simulation. If the compactness of protein is more then, the protein is more stable as shown in (Figure 3C).

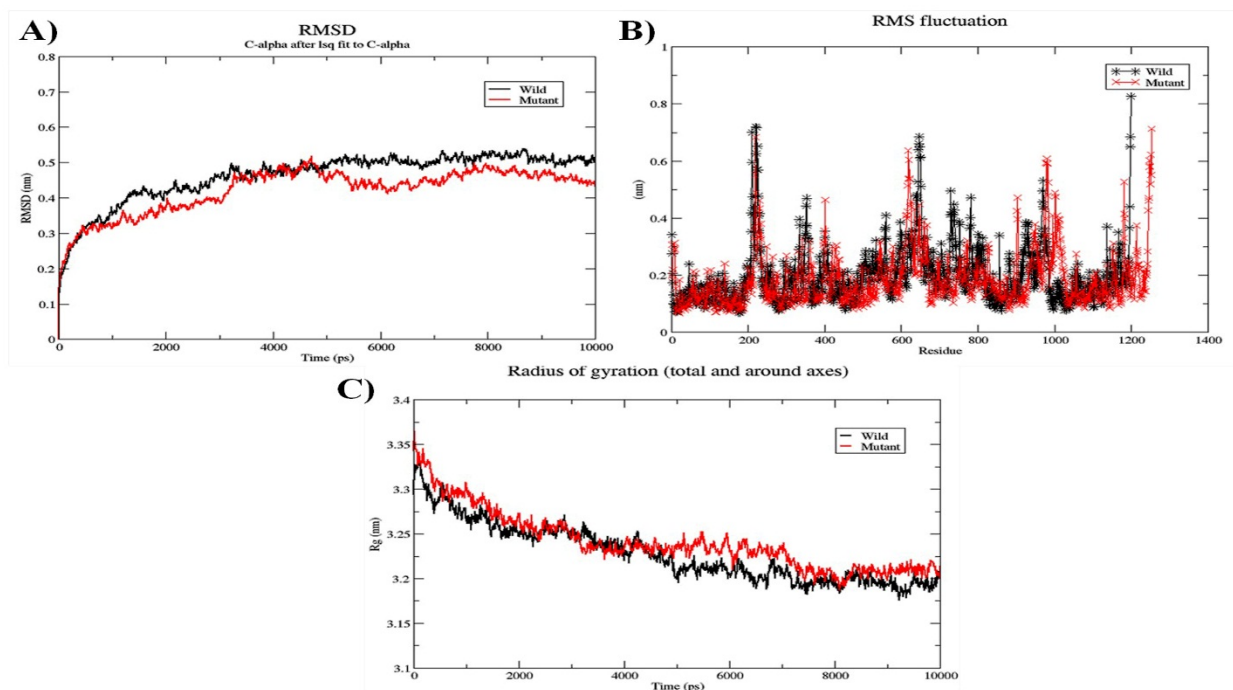


Fig 3. MD simulation analysis of wild and mutant (A) The RMSD plot of C-alpha atoms fluctuation of wild and mutant proteins (B) The fluctuation of protein residues throughout 10 ns simulation in RMSF plot (C) The compactness of both proteins during the simulation.

The intensive motion in trajectories through the eigenvectors of the covariance matrix of atomic fluctuation was studied with the help of PCA analyses. The dihedral angles i.e. Φ , Ψ of proteins were used to define the atomic fluctuation during simulation which was then taken to state the cosine content of the principal component of the covariance matrix. In general, the representative structure of a protein can be defined based on the cosine contribution of the first eigenvector. However, in many cases, the cosine contribution of the first eigenvector features large scale motion in protein dynamics. Thus, it cannot be used to depict protein behavior in terms of FEL. In recent studies, the first two PCs with cosine content values below 0.2 are considered to produce qualitatively related and smooth results. In the present study, the first 20 PCs of wild and mutant proteins were extracted and their cosine content was analyzed to find out the first two PCs having cosine content less than 0.2 as shown in (Figure 4 A and Figure 5 A). The coordinates of the first two PCs with such values were considered to construct the FEL plot. A single minimum energy cluster was observed in the 2D counter map of FEL of wild protein as shown in (Figure 4B). Based on the FEL 3D plot, the most representative structure of the minimum energy cluster was extracted as shown in (Figure 4C and D). Though there are two clusters in the 2D FEL counter map of the mutant protein, the lowest minimum energy cluster was attained from the 3D FEL plot as shown in (Figure 5B and C). The minimum energy structure of the mutant protein was extracted from the FEL counter map as shown in (Figure 5D).

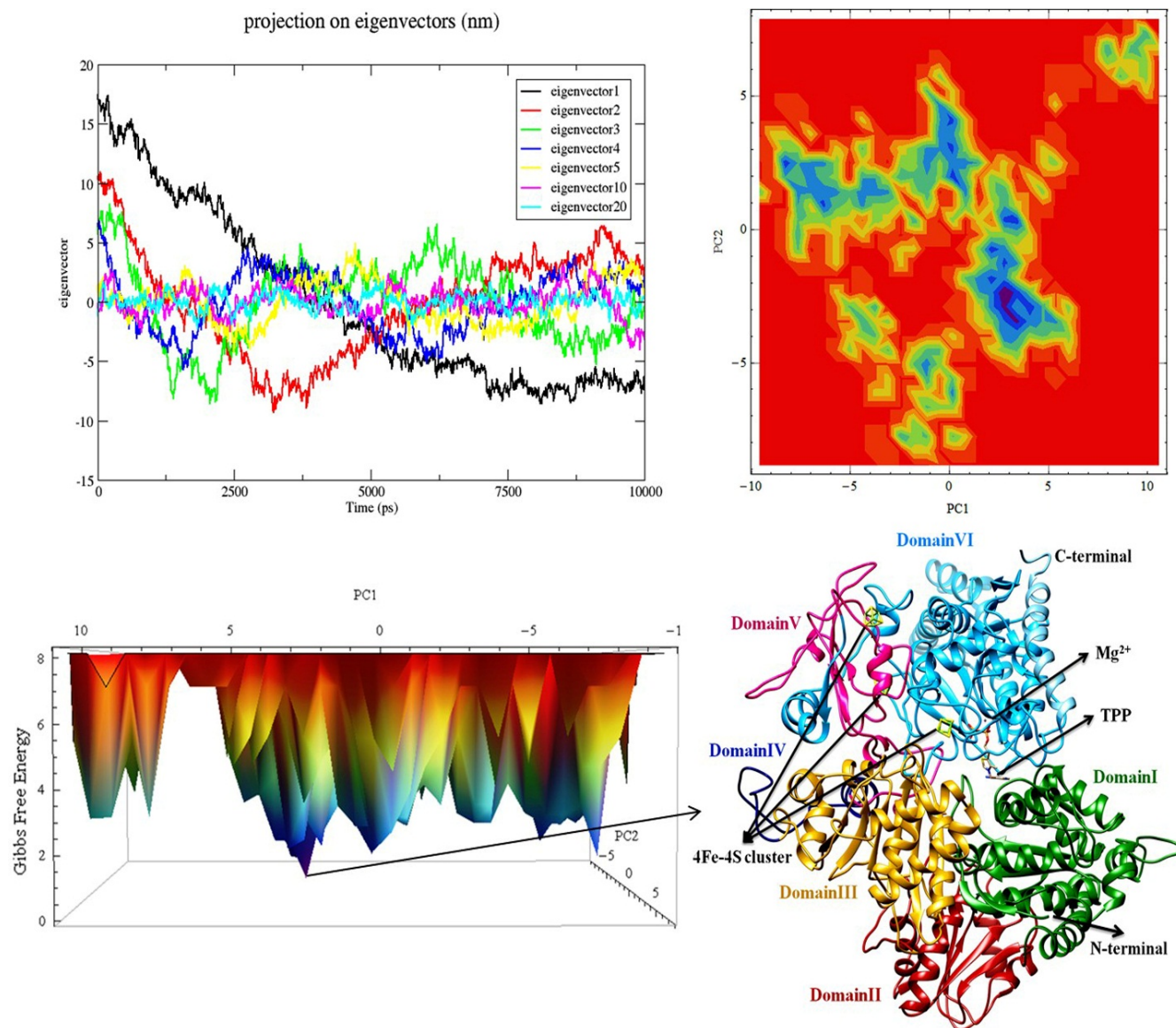


Fig 4. The essential dynamics analysis of the trajectory of wild protein. (A) The trajectory motion from the covariance matrix of wild protein (B) The 2D FEL counter map less than 0.2 (C) The 3D FEL plot (D) The minimum energy cluster extracted from the trajectory.

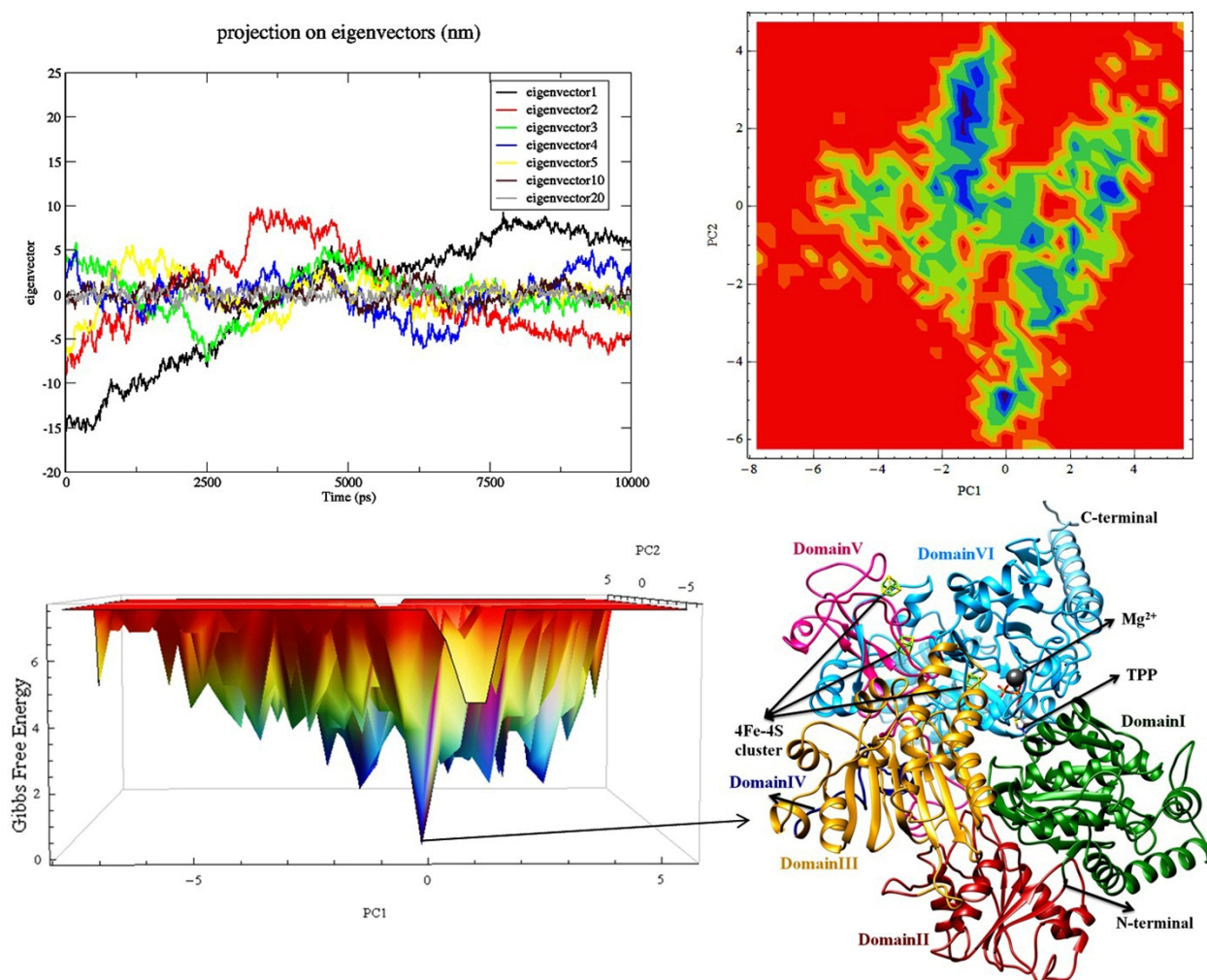


Fig 5. The essential dynamics analysis of the trajectory of the mutant protein. (A) The trajectory motion from the covariance matrix of the mutant protein (B) The 2D FEL counter map content less than 0.2 (C) The 3D FEL plot (D) The minimum energy cluster from the trajectory.

3.3 Prediction of the binding site for mutant and wild proteins

Since the binding site of 4-nitroimidazole is not yet known on these two proteins, it was predicted by CASTp server. It implements alpha shape method to identify topological features and to measure area and volume of pockets of protein to compute imprints. In wild protein, the predicted binding pockets residue numbers are 9, 12, 31, 35, 38-39, 42-46, 121, 123, 174, 178, 429-432, 434-435, 438-439, 442, 458, 462-466, 487, 494, 496, 551-552, 556, 560-563, 565, 599-600, 602-603, 606, 694-695, 770-771, 837, 1030-1032, 1046, 1049, 1106-1107, 1109-1113, 1158-1159, 1161-1162, 1165-1168. In case of mutant protein, the predicted binding pocket residue numbers are 14, 17, 35-36, 39-40, 43-44, 47, 119, 126-128, 179, 183, 379-382, 448-452, 454-455, 458-459, 476-480, 482-483, 485-486, 578-581, 614-620, 622-623, 626, 679-680, 682, 684, 704, 708, 713-715, 787, 789-795, 800, 802, 804, 857-858, 888, 892-895, 1071-1073, 1085-1087, 1090, 1148, 1151, 1153, 1156-1157.

3.4 4-nitroimidazole interaction with mutant and wild proteins

Among the six domains, the P-loop region of domain III i.e., 427-432 and Asn565, Asn607, Arg563, Phe596, Arg1046, Lys462, Thr31, and Asn1030 residues accommodates the coenzyme A (CoA) in wild protein. In the case of the mutant protein, the P-loop region that ranges from 447-452 and other residues such as Asn583, Asn627, Arg581, Tyr616, Arg1087, Lys482, Thr36, and Asn1071 interact with CoA.

In the docking studies, the compound 4-nitroimidazole formed H-bonds with Asp431, Gly432 (P-loop residues), Gly465 and Thr467 residues of domain III of wild protein and hydrophobic interaction with key residues i.e., Gly427, Met428, Ser430, Arg563 and Val433, Val434, Tyr458, Gly464, Phe466 and Ser493, as shown in (Figure 6 A). Unlike the wild and 4-nitroimidazole interaction which was sole with domain III residues, the mutant protein formed H-bonds with Ser450 (domain III), His736, Gly789 (domain V), Cys857 and Gly859 residues of domain VI. The compound had hydrophobic interactions with Lys481, Lys482, Ser483, Cys734, Pro735, Cys790, Ser856, Pro858, Cys860, Gly861, Leu1156, and Thr1157, as shown in (Figure 6B). The atoms involved in H-bond, the H-bond distance and hydrophobic interactions are written in Table 1.

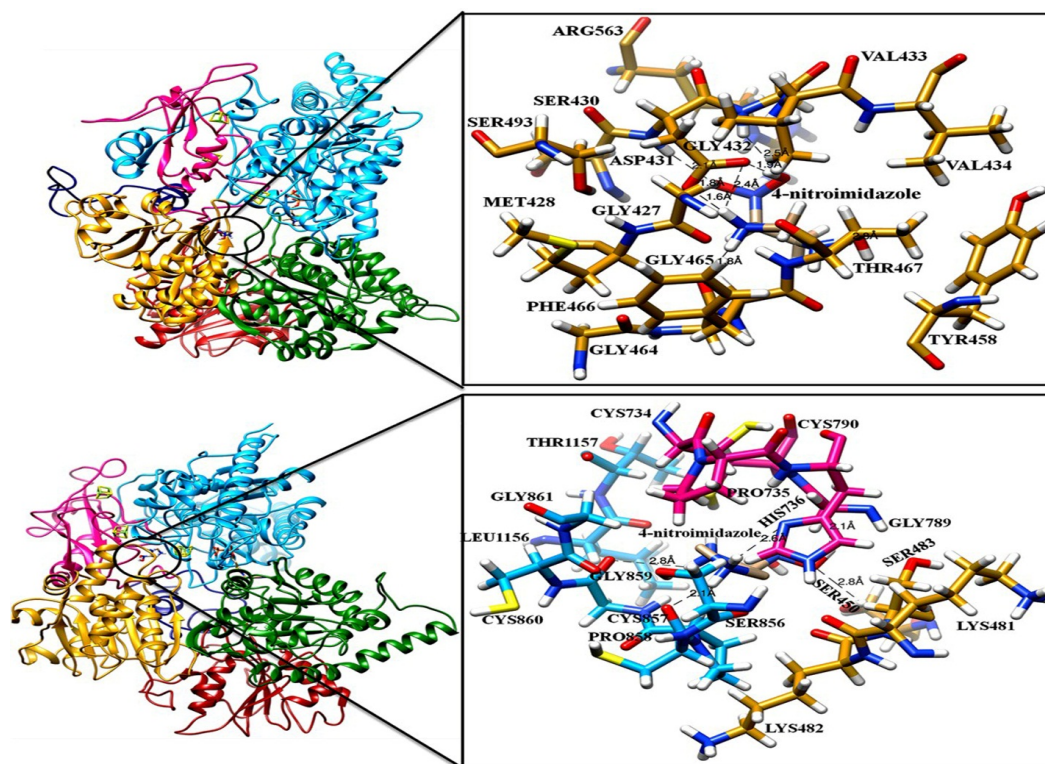


Fig 6. Molecular docking of 4-nitroimidazole with wild (above) and mutant (below) proteins. The docked pose (zoom out), H-bond and hydrophobic interactions (zoom in) of wild and mutant proteins.

Table 1. The atoms involved in H-bond between protein and 4-nitroimidazole, the H-bond distance and hydrophobic interaction.

Protein	4-nitroimidazole	H-bond distance (Å)	Hydrophobic interactions
Wild			
(H)	(O) UNK	2.1 Å	GLY427, MET428, SER430,
(OD1)	(H1) UNK	1.8 Å	VAL433, VAL434, TYR458,
ASP431 (OD1)	(H3) UNK	1.6 Å	GLY464, PHE466, SER493,
(OD2)	(HO) UNK	1.9 Å	ARG563
(OD2)	(H3) UNK	2.4 Å	
GLY432 (H)	(O) UNK	2.5 Å	
GLY465 (O)	(NH) UNK	1.8 Å	
THR467 (OG1)	(H2) UNK	2.8 Å	
Mutant			
SER450 (HG)	(O) UNK	2.8 Å	LYS481, LYS482, SER483, CYS734,
HIS736 (ND1)	(H2) UNK	2.6 Å	PRO735, CYS790, SER856,
GLY789 (O)	(HO) UNK	2.1 Å	PRO858, CYS860, GLY861,
CYS857 (O)	(HN) UNK	2.1 Å	LEU1156, THR1157
GLY859 (O)	(H) UNK	2.8 Å	

3.5 MD simulation analysis of mutant and wild complexes

Since the docking procedure is static, the complexes were further subjected to MD simulation analysis to understand the stability of H-bond interactions. As shown in Figure 7, the RMSD plot of both wild and mutant complexes was less than 0.4 nm. The major fluctuation in the RMSF graph of wild was seen at residue Val700 which is from structural linker (domain IV) followed by N- and C-terminal ends. Higher fluctuation at terminals is expected due to their free ends. The fluctuation of residues in the mutant complex was relatively less than the wild complex as shown in (Figure 7B). The compactness of both the complexes as per the Rg plot was more or less similar as shown in (Figure 7C). Since the stability of the compound is to be analyzed, H-bond plays an important role in the analysis. It can be observed in Figure 7D that wild complex maintained an approximate 4H-bonds during simulation while the mutant complex could hardly maintain single H-bond by the end of the simulation. This explains that 4-nitroimidazole is highly stable in wild complex rather than in the mutant complex.

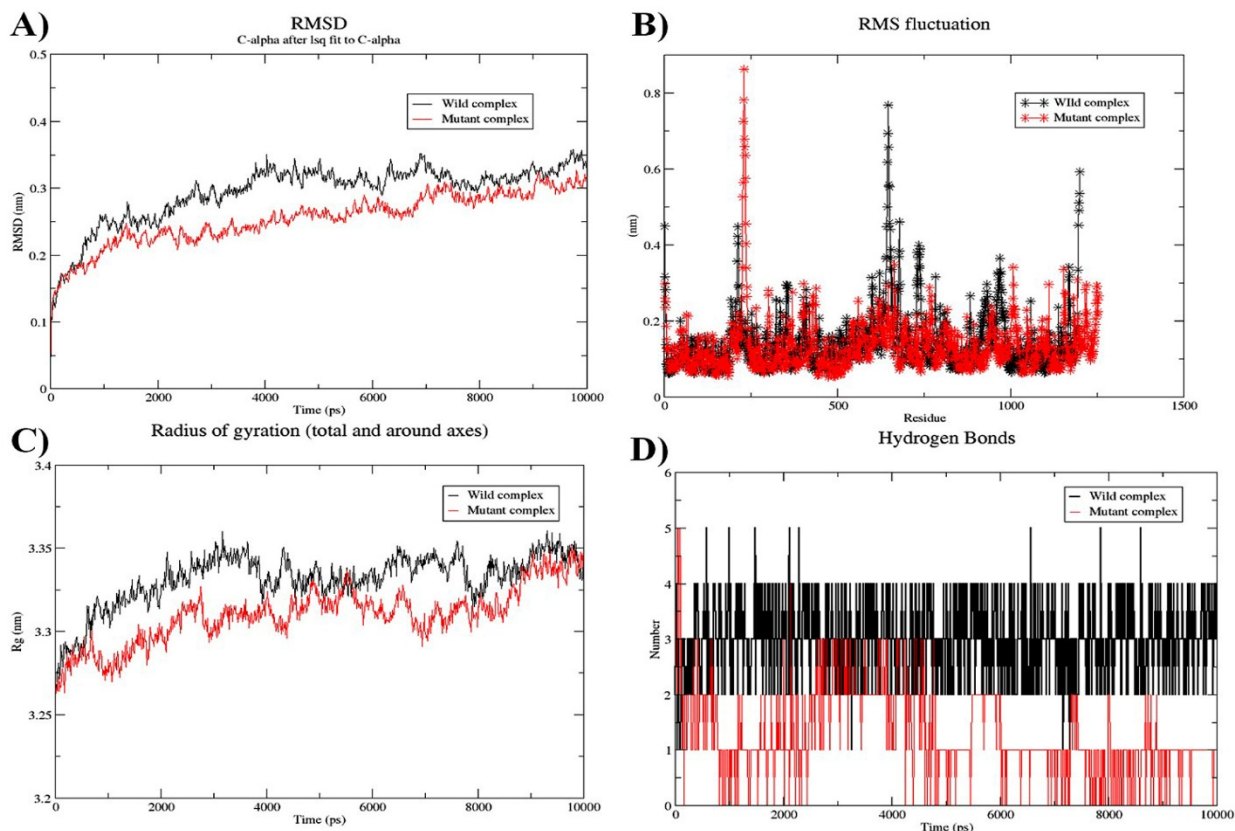


Fig 7. MD simulation analysis wild (black) and mutant (red) complexes (A) RMSD (B) RMSF (C) Radius of gyration (D) Number of H-bonds during 10ns simulation.

Although Figure 7 explains the higher number of H-bonds in wild complex, it does not elucidate the interacting residues and if new interactions are formed or not. Hence, clustering was performed for an entire trajectory with a cut-off of 0.1 to extract the most representative structure. The compound could maintain H-bond interactions with Asp431 (4 H-bonds) and Thr 467 while the rest of the residues from P-loop and Val433, Val434, Tyr458, Phe466, and Gly465 formed hydrophobic interaction. While in the mutant, the compound-maintained H-bond interaction with Cys857 and Gly859. The details of H-bond, its distance, and hydrophobic interactions are written in Table 2. As the compound 4-nitroimidazole could not make H-bond or hydrophobic interaction with key residues of the mutant protein, the compound may show less efficiency on mutant protein.

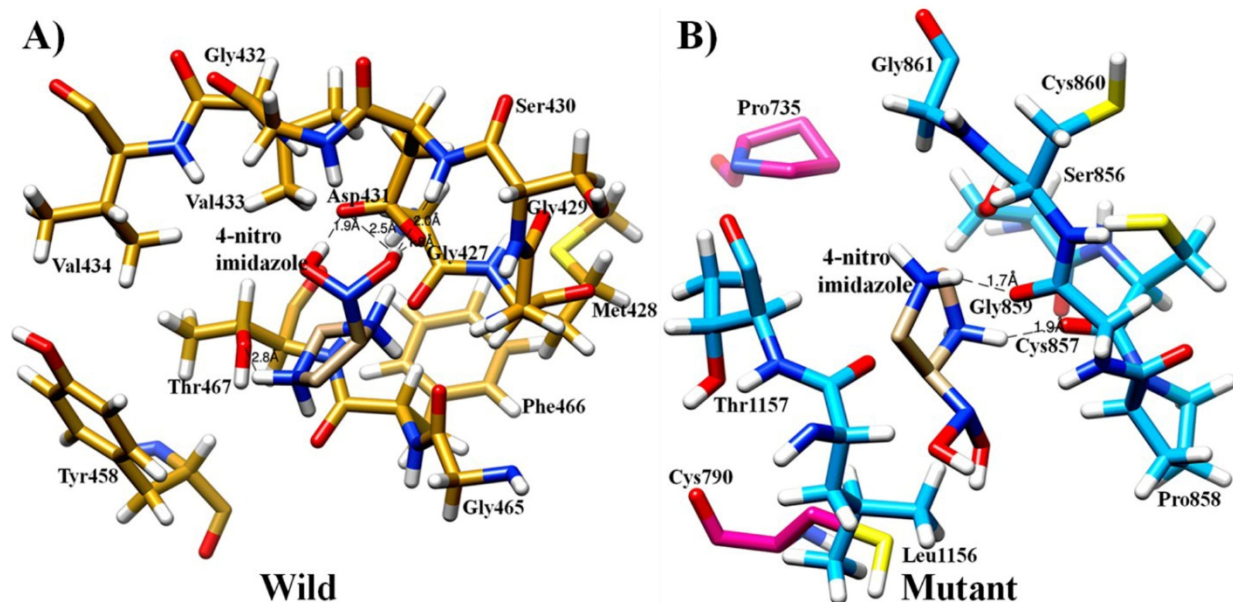


Fig 8. H-bond and hydrophobic interactions between (A) wild type (B) Mutant type and 4-nitroimidazole. The compound bound with P-loop residues of domain III in the wild while in the mutant, the interacting residues were from domain VI.

Table 2. The atoms involved in H-bond of protein-ligand complex, the H-bond distance and hydrophobic interaction after MD simulation.

Protein	4-nitro imidazole	H-bond distance (Å)	Hydrophobic interactions
Wild			
ASP431 (H)	(O) UNK	2.0 Å	GLY427, MET428, GLY429, SER430,
(OD1)	(H1) UNK	1.8 Å	GLY432, VAL433, VAL434, TYR458,
(OD2) (OD2)	(HO) UNK	1.9 Å	GLY465, PHE466
	(H1) UNK	2.5 Å	
THR467 (OG1)	(H2) UNK	2.8 Å	
Mutant			
CYS857 (O)	(H3) UNK	2.1 Å	PRO735, CYS790, SER856, PRO858,
GLY859 (O)	(H2) UNK	1.7 Å	CYS860, GLY861, LEU1156, THR1157

4 Discussion

Pyruvate Ferredoxin oxidoreductase is a protease enzyme that takes part in the synthesis pathway in some of the bacteria and parasites. The role of this enzyme is inactivation or inactivation some of the anti-parasite drugs, to date, this enzyme has not been crystallized. And thus, homology modeling was performed to predict the 3D protein structure using the Modeller9v19 script⁽²³⁾. On sequence alignments, it was observed that the sequence similarity between mutant strain and wild type is 51% and the protein structure of both the types can be modeled on the same template protein. To analyze the stability of the modeled structure and to extract the minimized structure, MD simulation was performed using GROMACS 5⁽²⁵⁾. All bonds pertained with LINear Constraint Solver (LINCS) holonomic constraints for van der Waals and electrostatic interactions with 10 Å cut-off⁽²⁶⁾. The binding site of both wild and mutant pyruvate ferredoxin oxidoreductase proteins was predicted by Computed Atlas of Surface Topography of proteins (CASTp) server. For long-range electrostatics, the Particle-Mesh-Ewald (PME) coulomb type with a cubic interpolation order of 4 and a grid spacing of 0.16 nm was applied⁽²⁷⁾. Finally, the MD run was performed in the NPT ensemble for a time scale of 10 ns. The same protocol was implemented for protein-ligand simulation while the ligand parameters were obtained from the swissparam server with CHARMM force field⁽²⁸⁾. Molecular docking was performed using AutoDock to predict the binding pocket of 4-nitroimidazole and to obtain its binding affinity⁽²⁹⁾. Both wild and mutant structures composed of six domains, three iron-sulfur [4Fe-4S] clusters, one thiamine pyrophosphate (TPP) and one Mg²⁺ molecule. In the root-mean-square fluctuation (RMSF) plot, the highest fluctuation was observed at C-terminus which generally

happens due to free end. As per the Rg plot, the compactness of both the proteins increased during the simulation. In the docking studies, the compound 4-nitroimidazole formed H-bonds with Asp431, Gly432 (P-loop residues), Gly465 and Thr467 residues of domain III of wild or PF1O protein and hydrophobic interaction with key residues i.e., Gly427, Met428, Ser430, Arg563 and Val433, Val434, Tyr458, Gly464, Phe466, and Ser493. The RMSD plot of both wild and mutant complexes was less than 0.4 nm. The major fluctuation in the RMSF graph of wild was seen at residue Val700 which is from structural linker (domain IV) followed by N- and C-terminal ends. It can be observed in that wild complex maintained an approximate 4H-bonds during simulation while the mutant complex could hardly maintain single H-bond by the end of the simulation. This explains that 4-nitroimidazole is highly stable in the wild complex rather than in the mutant complex. As the compound 4-nitroimidazole could not make H-bond or hydrophobic interaction with key residues of the mutant protein, the compound may show less efficiency on mutant protein.

5 Conclusion

The sequence similarity between wild type and mutant type is 51% and the 3D structure of both proteins could be built based on the same template protein. However, only mutant type is resistant to 4-nitroimidazole. The structural insights behind this resistance are unknown so far. In our study, the predicted tertiary structures of wild and mutant types were necessary to understand wild/mutant types 4-nitroimidazole interactions in computer-aided drug discovery procedures. This study predicts that 4-nitroimidazole may interrupt the binding of Co-A in wild type which is required for its regular function. Since the compound occupies this binding site by making stable H-bond with key interacting residues, the function of wild type may be affected. For the very reason, the mutant type may be resistant to the 4-nitroimidazole. Thus, this study predicted tertiary structures of wild and mutant types, the most probable binding site and also interacting residues of 4-nitroimidazole on both proteins. Besides, this study would be useful for the design derivatives of 4-nitroimidazole that inhibit protein function more efficiently.

Limitation

Nevertheless, the present study incorporated the suggested amino acid residues for site-directed drug-resistant results, so studies in vitro can be carried out to prove the above proposed in silico study.

Acknowledgments

The authors thank the Jawaharlal Institute of Postgraduate Medical Education and Research (JIPMER), Pondicherry, India for the financial support intramural Research Grant and also thank Dr. Pragnya from the Department of Bioinformatics, the University of Pondicherry for support and suggestion.

Conflict of Interest : The authors declare there are no competing interests

References

- 1) Ansell BRE, McConville MJ, Máayeh SY, Dagley MJ, Gasser RB, Svård SG, et al. Drug resistance in *Giardia duodenalis*. *Biotechnology Advances*. 2015;33:888–901. Available from: <https://dx.doi.org/10.1016/j.biotechadv.2015.04.009>.
- 2) Lane S, Lloyd D. Current Trends in Research into the Waterborne Parasite *Giardia*. *Critical Reviews in Microbiology*. 2002;28:123–147. Available from: <https://dx.doi.org/10.1080/1040-840291046713>.
- 3) McCormick B. Frequent symptomatic or asymptomatic infections may have long-term consequences on growth and cognitive development. In: Institute for Microbiology and Biochemistry Herborn. 2014;p. 23–39.
- 4) Kosek M, Bern C, Guerrant RL. The global burden of diarrhoeal disease. *Bulletin of the world health organization*. 1992;81:197–204. Available from: <https://www.scielosp.org/article/bwho/2003.v81n3/197-204/pt/>.
- 5) Savioli L, Smith H, Thompson A. *Giardia* and *Cryptosporidium* join the ‘Neglected Diseases Initiative’. *Trends in Parasitology*. 2006;22(5):203–208. Available from: <https://dx.doi.org/10.1016/j.pt.2006.02.015>.
- 6) Tian W, Chen C, Lei X, Zhao J, Liang J. CASTp 3.0: computed atlas of surface topography of proteins. *Nucleic Acids Research*. 2018;46(W1):W363–W367. Available from: <https://dx.doi.org/10.1093/nar/gky473>.
- 7) Verdu EF, Riddle MS. Chronic gastrointestinal consequences of acute infectious diarrhea: Evolving concepts in epidemiology and pathogenesis. *American Journal of Gastroenterology*. 2012;107(7):981–989. Available from: <https://dx.doi.org/10.1038/ajg.2012.65>.
- 8) Mørch K, Hanevik K, Rivenes AC, Bødtker JE, Næss H, Stubhaug B, et al. Chronic fatigue syndrome 5 years after giardiasis: differential diagnoses, characteristics and natural course. *BMC Gastroenterology*. 2013;13(1). Available from: <https://dx.doi.org/10.1186/1471-230x-13-28>.
- 9) Escobedo AA, Cimerman S. Giardiasis: a pharmacotherapy review. *Expert Opinion on Pharmacotherapy*. 2007;8:1885–1902. Available from: <https://dx.doi.org/10.1517/14656566.8.12.1885>.
- 10) Boreham PFL, Phillips RE, Shepherd RW. The sensitivity of *Giardia intestinalis* to drugs in vitro. *Journal of Antimicrobial Chemotherapy*. 1984;14(5):449–461. Available from: <https://dx.doi.org/10.1093/jac/14.5.449>.

- 11) McIntyre P, Boreham PFL, Phillips RE, Shepherd RW. Chemotherapy in giardiasis: Clinical responses and in vitro drug sensitivity of human isolates in axenic culture. *The Journal of Pediatrics*. 1986;108:1005–1010. Available from: [https://dx.doi.org/10.1016/s0022-3476\(86\)80950-7](https://dx.doi.org/10.1016/s0022-3476(86)80950-7).
- 12) Escobedo AA, Lalle M, Hrasnik NI, Rodríguez-Morales AJ, Castro-Sánchez E, Cimerman S, et al. Combination therapy in the management of giardiasis: What laboratory and clinical studies tell us, so far. *Acta Tropica*. 2016;162:196–205. Available from: <https://dx.doi.org/10.1016/j.actatropica.2016.06.026>.
- 13) Boreham PFL, Phillips RE, Shepherd RW. A comparison of the in-vitro activity of some 5-nitroimidazoles and other compounds against *Giardia intestinalis*. *Journal of Antimicrobial Chemotherapy*. 1985;16(5):589–595. Available from: <https://dx.doi.org/10.1093/jac/16.5.589>.
- 14) Čerkasovová A, Čerkasov J, Kulda J. Metabolic differences between metronidazole resistant and susceptible strains of *Tritrichomonas foetus*. *Molecular and Biochemical Parasitology*. 1984;11:105–118. Available from: [https://dx.doi.org/10.1016/0166-6851\(84\)90058-6](https://dx.doi.org/10.1016/0166-6851(84)90058-6).
- 15) Edwards DI. Nitroimidazole drugs-action and resistance mechanisms I. Mechanism of action. *Journal of Antimicrobial Chemotherapy*. 1993;31(1):9–20. Available from: <https://dx.doi.org/10.1093/jac/31.1.9>.
- 16) Leitsch D, Schlosser S, Burgess A, Duchêne M. Nitroimidazole drugs vary in their mode of action in the human parasite *Giardia lamblia*. *International Journal for Parasitology: Drugs and Drug Resistance*. 2012;2:166–170. Available from: <https://dx.doi.org/10.1016/j.ijpddr.2012.04.002>.
- 17) Gillin FD, Reiner DS. Effects of oxygen tension and reducing agents on sensitivity of *Giardia lamblia* to metronidazole in vitro. *Biochemical Pharmacology*. 1982;31(22):3694–3697. Available from: [https://dx.doi.org/10.1016/0006-2952\(82\)90600-1](https://dx.doi.org/10.1016/0006-2952(82)90600-1).
- 18) Müller J, Rout S, Leitsch D, Vaithilingam J, Hehl A, Müller N. Comparative characterisation of two nitroreductases from *Giardia lamblia* as potential activators of nitro compounds. *International Journal for Parasitology: Drugs and Drug Resistance*. 2015;5(2):37–43. Available from: <https://dx.doi.org/10.1016/j.ijpddr.2015.03.001>.
- 19) Müller J, Braga S, Heller M, Müller N. Resistance formation to nitro drugs in *Giardia lamblia*: No common markers identified by comparative proteomics. *International Journal for Parasitology: Drugs and Drug Resistance*. 2019;9:112–119. Available from: <https://dx.doi.org/10.1016/j.ijpddr.2019.03.002>.
- 20) Paget TA, Kelly ML, Jarroll EL, Lindmark DG, Lloyd D. The effects of oxygen on fermentation in *Giardia lamblia*. *Molecular and Biochemical Parasitology*. 1993;57:65–71. Available from: [https://dx.doi.org/10.1016/0166-6851\(93\)90244-r](https://dx.doi.org/10.1016/0166-6851(93)90244-r).
- 21) Müller J, Ley S, Felger I, Hemphill A, Müller N. Identification of differentially expressed genes in a *Giardia lamblia* WB C6 clone resistant to nitazoxanide and metronidazole. *Journal of Antimicrobial Chemotherapy*. 2008;62(1):72–82. Available from: <https://dx.doi.org/10.1093/jac/dkn142>.
- 22) Altschul SF, Gish W, Miller W, Myers EW, Lipman DJ. Basic local alignment search tool. *Journal of Molecular Biology*. 1990;215(3):403–410. Available from: [https://dx.doi.org/10.1016/s0022-2836\(05\)80360-2](https://dx.doi.org/10.1016/s0022-2836(05)80360-2).
- 23) Webb B, Sali A. Comparative Protein Structure Modeling Using MODELLER. *Current Protocols in Bioinformatics*. 2016;54(1):5–6. Available from: <https://dx.doi.org/10.1002/cpbi.3>.
- 24) Lovell SC, Davis IW, Arendall I, Wb D, Bakker PI, Word JM, et al. Structure validation by C α geometry: ϕ , ψ and C β deviation. *Proteins: Structure, Function, and Bioinformatics*. 2003;15(50(3)):437–450. Available from: <https://doi.org/10.1002/prot.10286>.
- 25) Spoel DVD, Lindahl E, Hess B, Groenhof G, Mark AE, Berendsen HJC. GROMACS: Fast, flexible, and free. *Journal of Computational Chemistry*. 2005;26(16):1701–1718. Available from: <https://dx.doi.org/10.1002/jcc.20291>.
- 26) Hess B, P-Lincs. A parallel linear constraint solver for molecular simulation. *Journal of chemical theory and computation*. 2008;4(1):116–122. Available from: <https://doi.org/10.1021/ct700200b>.
- 27) Wang H, Dommert F, Holm C. Optimizing working parameters of the smooth particle mesh Ewald algorithm in terms of accuracy and efficiency. *The Journal of Chemical Physics*. 2010;133. Available from: <https://dx.doi.org/10.1063/1.3446812>.
- 28) Zoete V, Cuendet MA, Grosdidier A, Michielin O. SwissParam: A fast force field generation tool for small organic molecules. *Journal of Computational Chemistry*. 2011;32(11):2359–2368. Available from: <https://dx.doi.org/10.1002/jcc.21816>.
- 29) Morris GM, Huey R, Lindstrom W, Sanner MF, Belew RK, Goodsell DS, et al. AutoDock4 and AutoDockTools4: Automated docking with selective receptor flexibility. *Journal of Computational Chemistry*. 2009;30(16):2785–2791. Available from: <https://dx.doi.org/10.1002/jcc.21256>.
- 30) Goodsell DS, Morris GM, Olson AJ. Automated docking of flexible ligands: Applications of autodock. *Journal of Molecular Recognition*. 1996;9:1–5. Available from: [https://dx.doi.org/10.1002/\(sici\)1099-1352\(199601\)9:1<1::aid-jmr241>3.0.co;2-6](https://dx.doi.org/10.1002/(sici)1099-1352(199601)9:1<1::aid-jmr241>3.0.co;2-6).
- 31) Morris GM, Huey R, Olson AJ. Using AutoDock for Ligand-Receptor Docking. *Current Protocols in Bioinformatics*. 2008;24:8–14. Available from: <https://dx.doi.org/10.1002/0471250953.bi0814s24>.